Rydberg hydrogen atom in the presence of uniform magnetic and quadrupolar electric fields

A quantum mechanical, classical and semiclassical approach

M. Iñarrea and J.P. Salas[a]

Area de Física Aplicada, Universidad de La Rioja, Logroño, Spain

Abstract. We present a quantum mechanical, classical and semiclassical study of the energy spectrum of a Rydberg hydrogen atom in the presence of uniform magnetic and quadrupolar electric fields. Here we study the case that the z-component P_ϕ of the canonical angular momentum is zero. In this sense, the dynamics depends on a dimensionless parameter λ representing the relative strengths of both fields. We consider that both external fields act like perturbations to the pure Coulombian system. In the classical study we find that, depending on the λ value, the phase flow shows four different regimes made up of vibrational and rotational trajectories, which are connected, respectively with the degenerate energy levels of double symmetry, and with the non-degenerate energy levels. The transit from one regime to another takes place by means of three oyster bifurcations. The semiclassical results are in good agreement with the results of the quantum mechanical calculations within the first-order perturbation theory. Moreover, we find that the evolution of the quantum/semiclassical energy spectrum can be explained by means of a classical description.

1 Introduction

The study of the dynamics of perturbed Rydberg atoms has been a very active field where classical and quantum mechanics shake hands often [1]. With this aim, and in order to complete a recent study performed in [2], here we consider the problem of a Rydberg hydrogen atom perturbed by a uniform magnetic field and a quadrupolar electric field. In that paper, an exhaustive study of the classical behaviour of the system, covering different aspects as integrability, parametric bifurcations and chaotic behaviour, has been done.

In the usual approximation for non-strong fields [3], the dynamics of the system is accurately governed by the following Hamiltonian [2,4]

$$\mathcal{H} = \frac{1}{2}\left(P_\rho^2 + P_z^2 + \frac{P_\phi^2}{2\rho^2}\right) - \frac{1}{\sqrt{\rho^2 + z^2}} - \gamma\, P_\phi$$
$$+ \frac{1}{2}\left[\left(\gamma^2 - \frac{w_z^2}{2}\right)\rho^2 + w_z^2 z^2\right], \quad (1)$$

where cylindrical coordinates (ρ, z, ϕ) and atomic units are used. In equation (1), P_ϕ is the z-component of the

ᵃ e-mail: josepablo.salas@dq.unirioja.es

canonical angular momentum, γ the Larmor frequency induced by the magnetic field and w_z the axial frequency induced by the quadrupolar electric field. Due to the axial symmetry, in Hamiltonian (1) P_ϕ is an integral, and (1) defines a two-dimensional dynamical system depending on the parameters P_ϕ, γ and w_z. As it is shown in [2], this system is in some cases equivalent to the one describing the generalised van der Waals interaction [5]. However, unlike the generalised van der Waals interaction, it can be considered as a real system describing a wider variety of dynamical situations.

Here in this paper we suppose that the Rydberg hydrogen atom is weakly perturbed by the magnetic and the quadrupolar fields. Under this assumption, we can treat the problem by using standard classical, quantum and semiclassical tools which provide a global vision of the dynamics of the system. We consider the $P_\phi = 0$ case.

The paper is organised as follows. In Section 2, by using classical perturbation theory, we compute an integrable approximation (*normal form*) to the original Hamiltonian. The dynamics arising from the normalised Hamiltonian is studied. This study involves the analysis of the stability of the equilibrium points, their bifurcations and the phase flow evolution. In Section 3, we calculate the quantum energy levels by means of first-order

quantum perturbation theory. In Section 4, we obtain the energy spectrum by semiclassical quantization of the normal form. We also compare the semiclassical results to those obtained quantically. Finally, in Section 5, the main results of the paper are summarised.

2 Classical perturbation theory

The Hamiltonian (1) may be written as the sum $\mathcal{H} = \mathcal{H}_0 + \mathcal{H}_1$ with

$$\mathcal{H}_0 = \frac{1}{2}(P_\rho^2 + P_z^2 + \frac{P_\phi^2}{2\rho^2}) - \frac{1}{\sqrt{\rho^2 + z^2}},$$

$$\mathcal{H}_1 = -\gamma P_\phi + \frac{1}{2}\left[(\gamma^2 - \frac{w_z^2}{2})\rho^2 + w_z^2 z^2\right], \qquad (2)$$

where the term $\mathcal{H}_0$ stands for the pure Coulombian system, while the term $\mathcal{H}_1$ describes the presence of the two external fields. Each negative value of $\mathcal{H}_0$ (bounded orbits) defines the semi-major axis $a = -1/2\mathcal{H}_0$ and the frequency $\widehat{w} = (-2\mathcal{H}_0)^{3/2}$ of a Keplerian orbit. When the effect of the external fields is taken as a perturbation to the pure Coulombian system, the trajectories of the electron can be described as Keplerian ellipses whose orbital parameters evolve under the influence of the perturbation. Following the Solove'v perspective [6], we assume that $\gamma \ll \widehat{w}$ and $w_z \ll \widehat{w}$. Under these conditions, the Hamiltonian $\mathcal{H}_1$ can be treated as a first order perturbation of $\mathcal{H}_0$. In this context, a normalization in the usual sense [7] allows us to reduce the problem to a integrable dynamical system where only one degree of freedom is left. To carry out this reduction, a Lie transformation [8] is sufficient. From the reduction, the new Hamiltonian admits the principal action (corresponding to the principal quantum number n) as an integral. As done for the Zeeman effect [9,10], for the Stark-Zeeman effect [11] and for the generalised van der Waals potential [12], we perform a Delaunay normalization [13] in the Keplerian action-angle variables $(I_1, I_2, I_3, \phi_1, \phi_2, \phi_3)$ [14]. The actions I_3, I_2 and I_1 are, respectively, the principal Delaunay variable (which corresponds to the principal quantum number n), the angular momentum (which corresponds to the quantum number l) and the z-component P_ϕ of the angular momentum (which corresponds to the the magnetic quantum number m). On the other side, the angles ϕ_3, ϕ_2 and ϕ_1 are, respectively, the mean anomaly, the argument of the perinucleus (the angle between the Runge-Lenz vector and the nodal line) and the angle between the angular momentum and the z-axis.

The Delaunay normalization is a canonical transformation

$$(I_1, I_2, I_3, \phi_1, \phi_2, \phi_3) \longrightarrow (I_1', I_2', I_3', \phi_1', \phi_2', \phi_3')$$

which converts $\mathcal{H}$ into a function $\mathcal{H}'$ that does not depend on the averaged mean anomaly ϕ_3'. By performing the reduction to the first order, and after dropping the primes

in the new variables, the normalised Hamiltonian (for the special case $I_1 = P_\phi = 0$) comes out as the sum

$$\mathcal{H}' = \mathcal{H}_0' + \mathcal{H}_1'$$

$$\mathcal{H}_0'(I_3) = -\frac{1}{2I_3^2},$$

$$\mathcal{H}_1'(\phi_2, I_2) = \frac{\gamma^2 I_3^4}{16}\left((2 + \lambda^2)(2 + 3e^2)\right.$$
$$\left. + 5(2 - 3\lambda^2)e^2 \cos 2\phi_2\right), \qquad (3)$$

where $e = \sqrt{1 - I_2^2/I_3^2}$ is the eccentricity of the Keplerian electronic orbits. Moreover, we have introduce the dimensionless parameter $\lambda = w_z/\gamma$ which represents the ratio between the Larmor frequency γ and the axial frequency w_z induced by the quadrupolar electric field. Note that in fact λ is representing the ratio between the strengths of the two external fields. As a consequence of $I_1 = 0$, the orbital plane is always perpendicular to the (x, y)-plane and it rotates around the z-axis with the (constant) Larmor frequency. Since I_3 is a constant of the motion in (3), the term $\mathcal{H}_0'$ can be neglected, and the normalised Hamiltonian $\mathcal{H}'$ reduces to $\mathcal{H}_1'$. Because $\mathcal{H}'$ has one degree of freedom, the phase trajectories are the maps of $\mathcal{H}'$ on the cylinders (ϕ_2, I_2). However, this representation do not cover the entire phase space, because they exclude the circular orbits $e = 0$ ($I_2 = I_3$). This singularity disappears [15] when the system is treated with the following variables

$$u = e \cos \phi_2, \quad v = e \sin \phi_2, \quad w = \pm\sqrt{1 - e^2} = \pm\frac{I_2}{I_3}. \quad (4)$$

It is worth noticing that (u, v) are the Cartesian components of the Runge–Lenz vector ($u^2 + v^2 = \mathbf{A}^2$, $v = A_z$), while w is the angular momentum I_2 divided by I_3. In this new map (u, v, w), given that

$$u^2 + v^2 + w^2 = 1,$$

the phase space consists of a unit radius sphere. In these coordinates, the points with $w > 0$ ($I_2 > 0$) stand for Keplerian ellipses travelled in a direct (prograde) sense, while those points with $w < 0$ ($I_2 < 0$) represent Keplerian ellipses travelled in a retrograde sense. Moreover, any point in the equatorial circle $w = 0$ ($I_2 = 0$) corresponds to a rectilinear orbit passing through the origin. Finally, the north (south) pole corresponds to circular orbits ($e = 0$) travelled in a direct (retrograde) sense. In coordinates (u, v, w) the Hamiltonian $\mathcal{H}' \equiv \mathcal{H}_1'$ becomes the function

$$\mathcal{H}' = \frac{\gamma^2 I_3^4}{8}\left[2 + \lambda^2 + (8 - 6\lambda^2)u^2 + (9\lambda^2 - 2)v^2\right]. \quad (5)$$

The Hamiltonian (5) indicates that the phase flow is time reversal symmetric with respect to the planes $u = 0$, $v = 0$ and $w = 0$. Consequently, the isolated equilibria, if any, must be $E_{1,2} = (\pm1, 0, 0)$, and/or on $E_{3,4} = (0, \pm1, 0)$ and/or on $E_{5,6} = (0, 0, \pm1)$. We shall also deduce this fact from the equations of the motion. In this way, taking

Table 1. Energy, stability and kind of orbit of the isolated equilibria.

Equilibrium	Energy	Stable when	Type of orbit
$E_{1,2} = (\pm 1, 0, 0)$	$\frac{5}{8}\gamma^2 I_3^4 (2 - \lambda^2)$	$\lambda \in [0,\ \sqrt{2/3}) \cup (2/\sqrt{3},\ \infty)$	linear orbits along $\pm\rho$
$E_{3,4} = (0, \pm 1, 0)$	$\frac{5}{4}\gamma^2 I_3^4 \lambda^2$	$\lambda \in [0,\ \sqrt{2}/3) \cup (\sqrt{2/3},\ \infty)$	linear orbits along $\pm z$
$E_{5,6} = (0, 0, \pm 1)$	$\frac{1}{8}\gamma^2 I_3^2 (\lambda^2 + 2)$	$\lambda \in [\sqrt{2}/3,\ 2/\sqrt{3}]$	circular orbits

into account the Jacobi-Liouville theorem and the Poisson brackets between the variables (u, v, w)

$$[u, v] = w, \qquad [v, w] = u, \qquad [w, u] = v,$$

the equations of motion associated to (5) are

$$\dot{u} = [u, \mathcal{H}_1'] = \frac{I_3^4}{4}(9\lambda^2 - 2)vw,$$

$$\dot{v} = [v, \mathcal{H}_1'] = \frac{I_3^4}{2}(3\lambda^2 - 4)uw, \qquad (6)$$

$$\dot{w} = [w, \mathcal{H}_1'] = \frac{5I_3^4}{4}(2 - 3\lambda^2)uv.$$

The equilibria of the reduced system are the solutions of the equations resulting of equating to zero the righthand members of the equations (6). It straightforward to see that, when λ is different from $(\pm\sqrt{2}/3, \pm\sqrt{2/3}, \pm 2/\sqrt{3})$ we arrive to the six mentioned (isolated) equilibria. Table 1 shows their corresponding energy, stability and type of orbit. We performed the stability analysis by studying the roots of the characteristic equation resulting from the variational equations of motion [16,17]. At the special cases of $\lambda = (\pm\sqrt{2}/3, \pm\sqrt{2/3}, \pm 2/\sqrt{3})$ we find that:

- when $\lambda = \sqrt{2}/3$, the number of isolated equilibria reduces to $E_{1,2}$ and it appears a circle of non-isolated equilibria along the meridian $v^2 + w^2 = 1$;
- when $\lambda = \sqrt{2/3}$, the number of isolated equilibria reduces to $E_{5,6}$ and it appears a circle of non-isolated equilibria along the meridian $u^2 + v^2 = 1$;
- when $\lambda = 2/\sqrt{3}$, the number of isolated equilibria reduces to $E_{3,4}$ and it appears a circle of non-isolated equilibria along the meridian $u^2 + w^2 = 1$.

This analysis indicates that the systems suffers three parametric bifurcations at the special values of $\lambda = (\pm\sqrt{2}/3,\ \pm\sqrt{2/3}, \pm 2/\sqrt{3})$. We can confirm the presence of bifurcations by studying the evolution, as a function of λ, of the energies of the equilibria (see Fig. 1). We observe in this figure that in the interval $0 \leq \lambda < \sqrt{2/3}$ the equilibria $E_{1,2}$ are absolute maxima. As a consequence of the Lyapunov theorem [17], these equilibria are always stable in this interval. For $\lambda > \sqrt{2/3}$ the absolute maximum is reached at the equilibria $E_{3,4}$ and then they are stable in this interval. On the other hand, the absolute minima is reached at the equilibria $E_{3,4}$ over the interval $0 \leq \lambda < \sqrt{2}/3$, at $E_{5,6}$ over $\sqrt{2}/3 < \lambda < \sqrt{2/3}$ and at $E_{1,2}$ for $\lambda > 2/\sqrt{3}$, in such a way that, by the Lyapunov theorem, they are also stable in the corresponding interval.
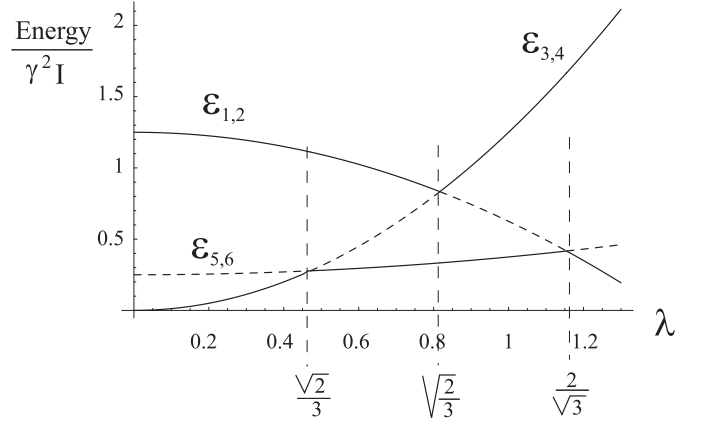

Fig. 1. Evolution of the values of the energy at the equilibria as a function of the parameter λ. Dashed lines indicates instability.

We observe that at $\lambda = \sqrt{2}/3$ the energy of the equilibria $E_{3,4}$ and $E_{5,6}$ is the same. A similar behaviour takes place for $E_{1,2}$ and $E_{3,4}$ at $\lambda = \sqrt{2/3}$, and for $E_{1,2}$ and $E_{5,6}$ at $\lambda = 2/\sqrt{3}$.

As we will find in Section 3, Figure 1 will be very useful in order to understand the quantum energy levels.

A detailed study of the behaviour of the system as a function of λ is provided by the phase flow evolution. In Figure 2 is shown the phase flow evolution on the cylinders (ϕ_2, I_2) — corresponding to Hamiltonian (3) — as well as the phase flow on the sphere — corresponding to Hamiltonian (4).

When $0 \leq \lambda < \sqrt{2}/3$, the phase flow is made of four families of contour lines (see Figs. 2a and 2b). In the (u, v, w) representation these families are kept apart by a separatrix passing through the unstable equilibria $E_{5,6}$. The equilibria E_1 and E_2 are located at $(\phi_2, I_2) = (0, 0)$ and $(\pi, 0)$, the equilibria E_3 and E_4 are located at $(\pi/2, 0)$ and $(3\pi/2, 0)$. Finally, the contour lines $I_2 = \pm I_3$ are, respectively, the equilibria E_5 and E_6. The two families of levels around the equilibria $E_{1,2}$ ($E_{3,4}$) correspond to quasiperiodic rotational $R_{1,2}$ (vibrational $V_{3,4}$) orbits oscillating around the linear orbits $E_{1,2}$ ($E_{3,4}$). A set of these orbits is depicted in Figure 3. For plotting Figure 3 we used the following procedure. Firstly, we take into account that every phase curve corresponds to a Keplerian ellipse whose eccentricity e evolves as the phase curve is gone over. The semi-major axis a is fixed by the energy of the phase curve. Hence, every point (ϕ_2, I_2) of the phase curve has associated a Keplerian ellipse whose cylindrical
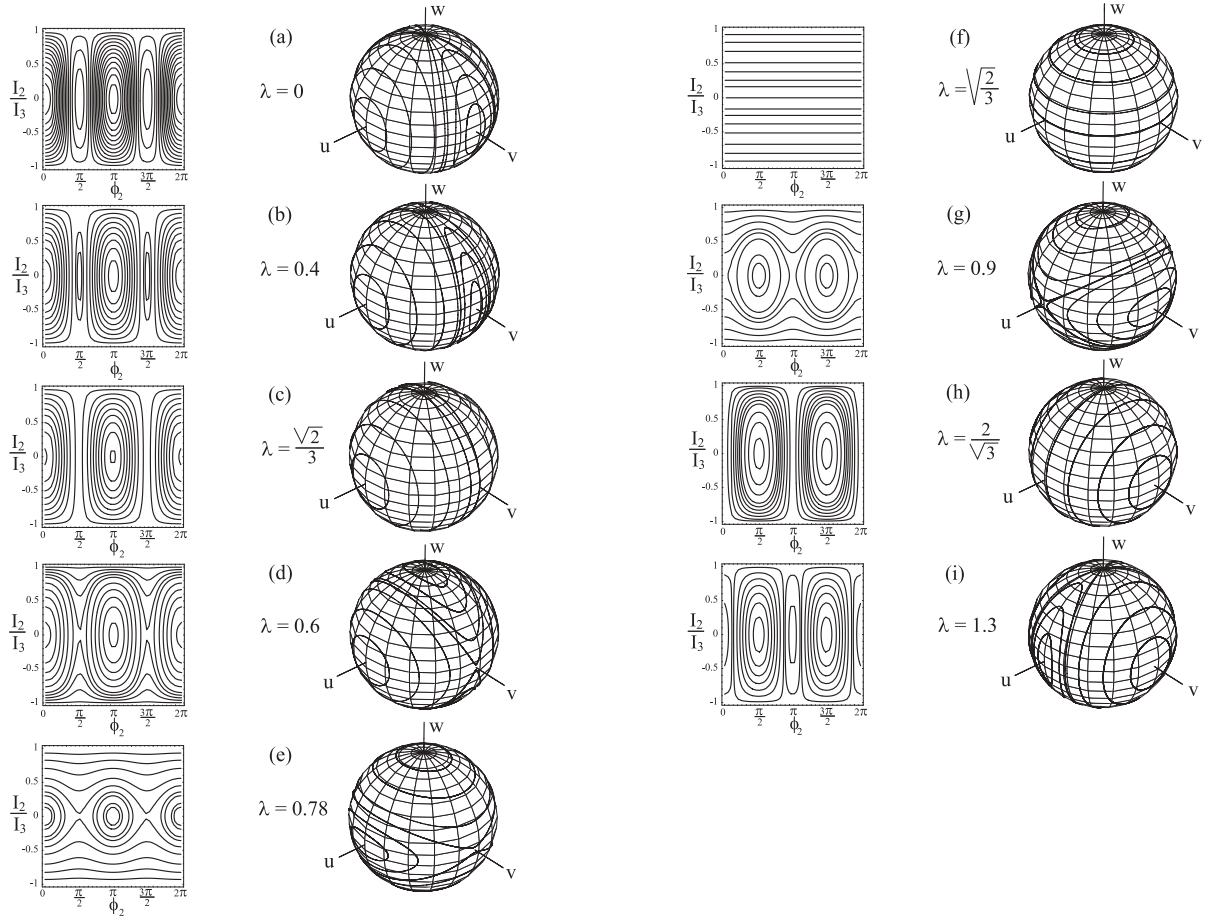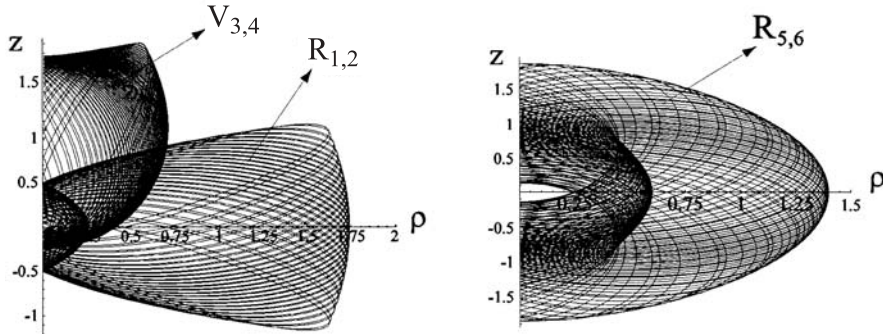
Fig. 2. Phase space evolution.

Fig. 3. Characteristic levels: rotational $R_{1,2}$, rotational $R_{5,6}$ and vibrational $V_{3,4}$.

coordinates (ρ, z) are given by

$$\rho = |r\cos\theta|, \qquad z = r\sin\theta,$$

$$r = \frac{a(1-e^2)}{1-e\cos(\phi_2-\theta)}, \qquad 0 \le \theta \le 2\pi. \qquad (7)$$

Note that, because of the symmetry properties of Hamiltonian (4), levels $R_{1,2}$ and $V_{3,4}$ occur always in pairs. However, it is important to note that when transformation (7) is applied to a pair of levels $R_{1,2}$, they become a unique rotational orbit in cylindrical coordinates. However, applied to a pair of vibrational levels $V_{3,4}$, they convert to different orbits in the (ρ, z) plane. Moreover, it is important to remark that, while for a rotational level R_1 or R_2 it is necessary to sweep the whole phase curve when (7) is applied, for a vibrational level V_3 or V_4 it is necessary to sweep only the halfway, because the other part would give the same values of (ρ, z). This fact will have capital importance for the semiclassical quantization in Section 4.

As λ approaches the value $\sqrt{2}/3$, the two homoclinic orbits of the separatrix tend to the meridian circle $v^2 + w^2 = 1$ (see Fig. 2b), in such a way that, when $\lambda = \sqrt{2}/3$ they meet one another along that meridian which becomes a circle of non-isolated equilibria for that value of λ (Fig. 2c). This is an example of a oyster

bifurcation. When the value $\sqrt{2}/3$ is crossed, a new separatrix passing through $E_{3,4}$ opens its lobes (see Fig. 2d).

As a consequence of this bifurcation, the equilibria $E_{3,4}$ and $E_{5,6}$ switch their stability, the vibrational levels $V_{3,4}$ disappear and two new families of levels appear around the equilibria $E_{5,6}$. This new kind of levels (named as $R_{5,6}$) is associated to quasiperiodic orbits oscillating around the circular orbits $E_{5,6}$ (see Fig. 3). These levels correspond also to rotational motion. In fact, in a pendulum or rotor picture, levels $R_{5,6}$ would correspond to a genuine rotational motion where the rotor or pendulum is describing complete rotations. Note that, for a given energy, the corresponding rotational levels $R_{5,6}$ are equivalent because they represent the same orbit travelled in direct (around E_5) or retrograde sense (around E_6).

In the interval $\sqrt{2}/3 < \lambda < \sqrt{2/3}$, the homoclinic lobes tend to the equator as λ approaches $\sqrt{2/3}$ (see Fig. 2e), in such a way that, for $\lambda = \sqrt{2/3}$, the equator is a circle of non-isolated equilibria and the phase flow is made of rotational levels $R_{5,6}$ (see Fig. 2f). A second oyster bifurcation takes place. As a consequence of this bifurcation, the equilibria $E_{1,2}$ and $E_{3,4}$ exchange their stability, the separatrix passes now through the equilibria $E_{1,2}$ and the phase flow is made of vibrators ($V_{3,4}$) around $E_{3,4}$ and rotators $R_{5,6}$ around $E_{5,6}$ (see Fig. 2g). In the interval $\sqrt{2/3} < \lambda < 2/\sqrt{3}$ the separatrix lobes tend to the meridian $u^2 + w^2 = 1$ in such a way that a third oyster bifurcation takes place along that meridian at $\lambda = 2/\sqrt{3}$. Note that, for $\lambda = 2/\sqrt{3}$, the phase flow consists of only vibrational levels $V_{3,4}$ (see Fig. 2h). For $\lambda > 2/\sqrt{3}$ the equilibria $E_{1,2}$ and $E_{5,6}$ switch their stability, and the phase flow has the same structure than in the interval $\lambda < \sqrt{2}/3$.

3 Quantum perturbation theory

When the external fields are perturbations, their effect on the energy spectrum of the hydrogen atom may be calculated by using first-order degenerate perturbation theory. From a qualitative point of view, this assumption holds when the perturbations strengths γ and λ are smaller than the energy spacing between consecutive hydrogenic manifolds, i.e.,

$$\gamma^2 n^7 \ll 1, \qquad w_z^2 n^7 \ll 1.$$

Hence, for a given n-manifold, the eigenstates of (1) for $m = 0$ can be expressed as a function of the pure hydrogenic basis by using the following expansion over the orbital quantum number l

$$\Psi_{n,k}(r,\theta) = \sum_{l=0}^{n-1} c_l^{nk} R_{nl}(r) Y_l^0(\theta,0), \quad k = 0,...,n-1, \quad (8)$$

since n remains a good quantum number within the first-order theory. The values of coefficients c_l^{nk} follow after solving the secular problem for the perturbation, which involves the diagonalization of a matrix obtained by representing the operators $\rho^2 = r^2 \sin^2 \theta$ and $z^2 = r^2 \cos^2 \theta$
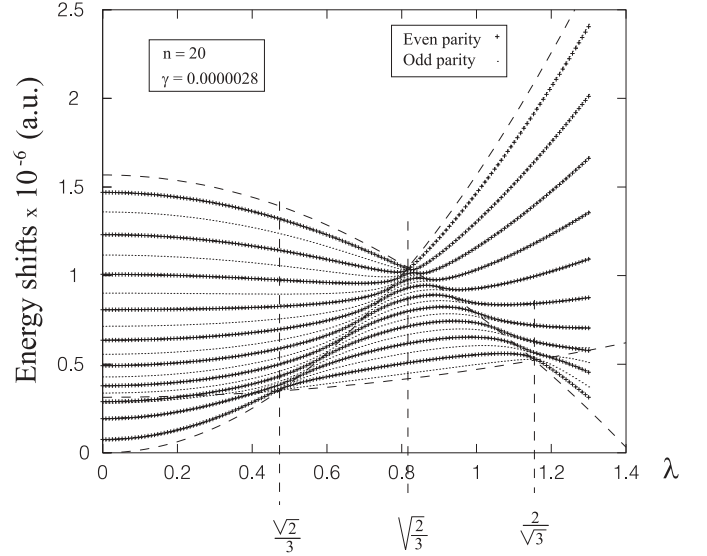

Fig. 4. Energy-level shifts of the $n = 20$ manifold for $\gamma \approx 2.8 \times 10^{-6}$ as a function of λ. Dashed lines represent the energy evolution of the classical equilibria for the same values of the parameters.

in the hydrogenic basis $\{|nlm\rangle; l = 0,...,n-1; m = 0\}$. We note that, because $\mathcal{H}$ commutes with the parity operator Π, each eigenstate $\Psi_{n,k}(r,\theta)$ has the same definite parity as the corresponding unperturbed eigenstate. From (1), the required matrix elements are

$$\frac{\gamma^2}{2}[(1 - \frac{\lambda^2}{2})\rho_{ll'}^2 + \lambda^2 z_{ll'}^2] \qquad (9)$$

being

$$
\begin{aligned}
\rho_{ll'}^2 &= \langle nl0|\rho^2|nl'0\rangle \\
&= -\frac{5n^2}{2}(l+2)(l+1)\sqrt{\frac{(n^2-(l+2)^2)(n^2-(l+1)^2)}{(2l+5)(2l+3)^2(2l+1)}}\delta_{l,l'+2} \\
&\quad + \frac{n^2[5n^2+1-3l(l+1)](l^2+l-1)}{(2l-1)(2l+3)}\delta_{l,l'} \\
&\quad - \frac{5n^2}{2}\sqrt{(n^2-l^2)(n^2-(l-1)^2)} \\
&\quad \times \frac{l(l-1)}{\sqrt{(2l+1)(2l-1)^2(2l-3)}}\delta_{l,l'-2} \qquad (10)
\end{aligned}
$$

$$
\begin{aligned}
z_{ll'}^2 &= \langle nl0|z^2|nl'0\rangle \\
&= \frac{n^2}{2}[5n^2+1-3l(l+1)]\delta_{l,l'} - \langle nl0|\rho^2|nl'0\rangle.
\end{aligned}
$$

If we denote the eigenvalues (energy shifts) of the matrix (9) by $\Delta E_{n,l}(\gamma, \lambda)$, the energy levels are

$$E_{n,l} = -1/2n^2 + \Delta E_{n,l}(\gamma, \lambda).$$

Both parities energy-level shifts (in atomic units) for the $n = 20$ manifold and $\gamma = 1/10n^{7/2} \approx 2.8 \times 10^{-6}$ in the range $\lambda \in [0, 1.3]$ are shown in Figure 4. In this figure and for the same values of γ and n (i.e., I_3), it is superimposed

the evolution of the energy of the classical equilibria obtained in Section 2. We observe in this figure that the energies of the classical equilibria act like the enveloping of the quantum spectrum, in such a way that the quantum spectrum presents three zones of accumulations (strong degeneration) around the values of $\lambda = (\sqrt{2}/3, \sqrt{2/3}, 2/\sqrt{3})$ for which the classical system suffers the three bifurcations. In other words, the evolution of the energies of the classical equilibria is a some kind of sketch of the evolution of the quantum spectrum.

Finally, the mentioned parallelism between classical-quantum energy behaviour proves again that classical mechanics is a powerful tool which provides a compact description of the energy level structure of the perturbed Rydberg atoms.

4 Semiclassical quantization

As we have seen in Section 2, the classical normalised system (3) is integrable, therefore the semiclassical energy levels can be calculated by means of the so–called Einstein–Brillouin–Keller (EBK) quantization rules [18]. From the semiclassical point of view, each regular trajectory having appropriately quantized values of the action variables corresponds to a quantum state. Such trajectories are usually called the *eigentrajectories*. More exactly, the whole class of the trajectories confined on an invariant torus determined by quantized values of the action variables is that which corresponds to a quantum state [19]. However, we can take an arbitrary trajectory on the torus as representative. In the problem at hand, the normal form (3) can be quantized by applying the EBK rules to the action-angle variables $(I_1, I_2, I_3, \phi_1, \phi_2, \phi_3)$ [20]. Expressed in these variables, the Hamiltonian $\mathcal{H}'_1$ takes the form

$$
\begin{aligned}
\epsilon \equiv {}& \mathcal{H}'_1(\phi_2, I_2) \\
={}& \frac{\gamma^2 I_3^4}{16} \left\{ (2 + \lambda^2) \left[2 + 3 \left(1 - \frac{I_2^2}{I_3^2} \right) \right] \right. \\
& \left. + 5(2 - 3\lambda^2) \left(1 - \frac{I_2^2}{I_3^2} \right) \cos 2\phi_2 \right\}.
\end{aligned} \quad (11)
$$

In the above expression I_1 and I_3 are, respectively, exact and approximate constants of the motion and they can be quantized as in the unperturbed hydrogen atom

$$
I_1 = m = 0, \qquad I_3 = n, \quad (12)
$$

where m is the magnetic quantum number and n is the principal quantum number. However, because of the presence of the perturbations, the angular momentum I_2 is not a constant of the motion, and the action which has to be quantized is the following [21]

$$
A = \frac{1}{2\pi} \oint_C I_2 \, d\phi_2 = k + \frac{1}{2}, \qu(13)
$$

where $I_2(\phi_2, \mathcal{H}_1)$ appears after solving equation (11) for I_2. A similar strategy for the semiclassical quantization has been followed in the study of the Zeeman effect [22], the Zeeman-Stark effect [23] and the instantaneous [24] and generalised [25] van der Waals interaction.

In Section 2 we saw that, depending on the value of λ, we find four different phase flows. The evolution from one to another is *via* three oyster bifurcations for $\lambda = (\sqrt{2}/3, \sqrt{2/3}, 2/\sqrt{3})$. Through these bifurcations, the six equilibria interchange their stability, which gives rise to different kind of trajectories. When this phase flow evolution is considered in the cylinders (ϕ_2, I_2), trajectories are sorted in two main categories: the vibrational trajectories (V_3, V_4), and the rotational trajectories (R_1, R_2) inside the separatrix and (R_5, R_6) outside the separatrix.

In Section 2 we noted that every pair of levels $R_{1,2}$ represents the same orbit in the real space (ρ, z). Therefore, to obtain the corresponding semiclassical spectrum, we must apply the rule (13) either to levels R_1 or to levels R_2. Hence, applying (13) to levels R_1, the action integral A is $1/2\pi$ times the area enclosed by a given rotational orbit R_1. We also noted that every pair of vibrational half-loops $V_{3,4}$ represents different orbits in the plane (ρ, z), in such way that (13) has to be applied to both levels V_3 and V_4. In this case, the action integral A is $1/2\pi$ times the area enclosed between a given vibrational contour line V_3 (V_4) and the line $I_2 = 0$. Finally, because every pair of rotational trajectories $R_{5,6}$ is the same orbit travelled in opposite senses, the action integral A can be obtained as $1/2\pi$ times the area enclosed by a given orbit R_5 and the line $I_2 = 0$.

Now, in order to apply the semiclassical rule (13), let us consider separately the aforementioned four phase flow regimes.

For $0 \leq \lambda < \sqrt{2}/3$, the energy ϵ takes values $\epsilon_{3,4} \leq \epsilon \leq \epsilon_{1,2}$ and the energy at the separatrix is $\epsilon_s = \epsilon_{5,6}$ (see Tab. 1 and Fig. 1). The phase space consists of a double family of vibrational trajectories (V_3, V_4) around $E_{3,4}$, and another double family of rotational orbits (R_1, R_2) around $E_{1,2}$. These two double families are divided by the separatrix passing through $E_{5,6}$ (see Figs. 2a and 2b). Taking into account the symmetries of the (ϕ_2, I_2) phase space, the action integral A for vibrational motions (V_3, V_4) is given by

$$
\begin{aligned}
A_{V_3, V_4} ={}& \frac{1}{\pi \gamma I_3} \mathcal{J}(\epsilon) \\
={}& \frac{1}{\pi \gamma I_3} \int_{\phi_2^0}^{\pi/2} \sqrt{\frac{5\gamma^2 I_3^4 [2 + \lambda^2 - (3\lambda^2 - 2) \cos 2\phi_2] - 16\epsilon}{3(2 + \lambda^2) - 5(3\lambda^2 - 2) \cos 2\phi_2}} \, d\phi_2, \\
& \epsilon_{3,4} < \epsilon < \epsilon_{5,6}, \quad (14)
\end{aligned}
$$

while for the rotational orbits R_1, it results

$$
\begin{aligned}
A_{R_1} ={}& \frac{1}{\pi \gamma I_3} \mathcal{J}(\epsilon) \\
={}& \frac{2}{\pi \gamma I_3} \int_0^{\phi_2^0} \sqrt{\frac{5\gamma^2 I_3^4 [2 + \lambda^2 - (3\lambda^2 - 2) \cos 2\phi_2] - 16\epsilon}{3(2 + \lambda^2) - 5(3\lambda^2 - 2) \cos 2\phi_2}} \, d\phi_2, \\
& \epsilon_{5,6} < \epsilon < \epsilon_{1,2}, \quad (15)
\end{aligned}
$$

where $\phi_2^0 = \frac{1}{2} \arccos\left[\frac{1}{3\lambda^2 - 2} \left(2 + \lambda^2 - \frac{16\epsilon}{5\gamma^2 I_3^4} \right) \right]$.

For $\lambda = \sqrt{2}/3$, the first bifurcation, the energy ϵ takes values $\epsilon_{3,4} = \epsilon_{5,6} \le \epsilon \le \epsilon_{1,2}$ (see Tab. 1 and Fig. 1). The phase flow is only made of the double family of rotational orbits (R_1, R_2) around the equilibria $E_{1,2}$ (see Fig. 2c). In this case, the action integral A for the rotational motion R_1 is the same as (15).

For $\sqrt{2}/3 \le \lambda < \sqrt{2/3}$, the energy $\epsilon \in [\epsilon_{5,6}, \epsilon_{1,2}]$ and the energy at the separatrix is $\epsilon_s = \epsilon_{3,4}$ (see Tab. 1 and Fig. 1). In this case, the phase space consists of the double family of rotational trajectories (R_1, R_2) under the separatrix, and another family of rotational orbits R_5, R_6 above the separatrix passing through the unstable equilibria $E_{3,4}$ (see Figs. 2d and 2e). Taking into account the symmetries of the phase space, for the rotational motion R_5, the action integral A is

$$A_{R_5} = \frac{1}{\pi \gamma I_3} \mathcal{J}(\epsilon)$$

$$= \frac{1}{\pi \gamma I_3} \int_{-\pi/2}^{\pi/2} \sqrt{\frac{5\gamma^2 I_3^4 [2 + \lambda^2 - (3\lambda^2 - 2)\cos 2\phi_2] - 16\epsilon}{3(2 + \lambda^2) - 5(3\lambda^2 - 2)\cos 2\phi_2}} \, d\phi_2,$$

$$\epsilon_{5,6} < \epsilon < \epsilon_{3,4}, \quad (16)$$

whereas for the rotational trajectories R_1, the integral A is the same as (15) with $\epsilon_{3,4} < \epsilon < \epsilon_{1,2}$.

For $\lambda = \sqrt{2/3}$, the second bifurcation, the energy ϵ takes values $\epsilon_{5,6} \le \epsilon \le \epsilon_{1,2} = \epsilon_{3,4}$ (see Tab. 1 and Fig. 1). The phase flow is only made of the rotational orbits (R_5, R_6) around the equilibria $E_{5,6}$ (see Fig. 2f). Therefore, in this case the action integral A for these rotational trajectories is given by (16).

For $\sqrt{2/3} \le \lambda < 2/\sqrt{3}$, the energy $\epsilon \in [\epsilon_{5,6}, \epsilon_{3,4}]$ and the energy at the separatrix is $\epsilon_s = \epsilon_{1,2}$ (see Tab. 1 and Fig. 1). Now, the phase space consists of the double family of vibrational orbits (V_3, V_4) and the family of rotational trajectories (R_5, R_6) outside the separatrix passing in this case through the equilibria $E_{1,2}$ (see Fig. 2g). The action integral A results in (14) with $\epsilon \in (\epsilon_{1,2}, \epsilon_{3,4})$ for the vibrational orbits, while for the rotational ones A is the same as (16) with $\epsilon \in (\epsilon_{5,6}, \epsilon_{1,2})$.

For $2/\sqrt{3}$, the third bifurcation, the energy ϵ takes values $\epsilon_{1,2} = \epsilon_{5,6} \le \epsilon \le \epsilon_{3,4}$ (see Tab. 1 and Fig. 1). The phase flow is only made of the double family of vibrational orbits (V_3, V_4) (see Fig. 2h). In this case, the action integral A for these vibrational trajectories yields (14) with $\epsilon \in (\epsilon_{1,2}, \epsilon_{3,4})$.

Finally, for $\lambda > 2/\sqrt{3}$, the energy $\epsilon \in [\epsilon_{1,2}, \epsilon_{3,4}]$ and the energy at the separatrix is $\epsilon_s = \epsilon_{5,6}$ (see Tab. 1 and Fig. 1). Again, the phase flow consists of the double family of vibrational trajectories (V_3, V_4), and the double family of rotational orbits (R_1, R_2). These two double families are kept apart by the separatrix passing through equilibria $E_{5,6}$ (see Fig. 2i). For the R_1 rotational motions, the action integral A is given by (15) with $\epsilon_{1,2} < \epsilon < \epsilon_{5,6}$, whereas for the (V_3, V_4) vibrational orbits A results in (14) with $\epsilon_{5,6} < \epsilon < \epsilon_{3,4}$.

In order to obtain the semiclassical energy levels $E_{n,k}$ of the system for any given quantized values k and n, the application of the EBK rules (12) and (13), yields the
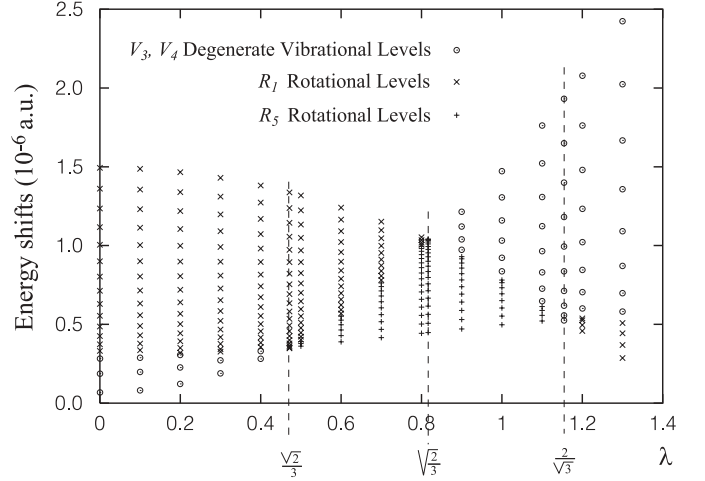

Fig. 5. Semiclassical energy-level shifts of the $n = 20$ manifold for $\gamma \approx 2.8 \times 10^{-6}$ as a function of λ.

following equation

$$\mathcal{J}(\epsilon) = \pi \, n \, \gamma \left(k + \frac{1}{2} \right), \quad (17)$$

where $\mathcal{J}(\epsilon)$ are the integrals appearing in (14), (15) and (16) with the adequate limits for ϵ depending on the value of λ. We have solved equation (17) by means of an appropriate numerical bisection procedure for finding zeros, combined with the numerical integration of $\mathcal{J}(\epsilon)$. If we label the solution of (17) with $\epsilon_{n,k}$ (the energy-level shifts), we get the following semiclassical energy formula

$$E_{n,k} = -\frac{1}{2n^2} + \epsilon_{n,k}. \quad (18)$$

In Tables 2 and 3 are shown, for $n = 20$, $\gamma \approx 2.8 \times 10^{-6}$ and eight different values of λ in the range $\lambda \in [0, 1.3]$, the semiclassical energy-level shifts together with the corresponding quantum-mechanical results from Section 3. Note that the $n = 20$ manifold consists of twenty semiclassical states because the vibrational levels corresponding to the states (V_3, V_4) are always doubly degenerate. It can be seen that the semiclassical results are in very good agreement with the quantum-mechanical ones. The tiny splitting of the degeneracy appearing for the quantum-mechanical values of the vibrational energy levels near the classical separatrix is due to a tunnelling between vibrational states V_3 and V_4 in the vicinity of the separatrix. This splitting does not appear in the semiclassical energy levels because the semiclassical EBK rules do not incorporate quantum-mechanical tunnelling effects. Figure 5 shows the semiclassical energy-level shifts appearing in the aforementioned tables. In this figure we have depicted with different symbols the energy shifts corresponding to different types of classical orbits. As was to be expected, Figure 5 is an accurate sketch of Figure 4.

In some cases (e.g. for $\lambda = 0.3$ in Tab. 2 and for $\lambda = 1.0$ in Tab. 3) we have obtained from the solution of equation (17) only $n - 1$ levels instead of n for

Table 2. Energy-level shifts of the $n = 20$ manifold for $\gamma \approx 2.8 \times 10^{-6}$ and different values of λ. Comparison between the semiclassical and quantum-mechanical results. k: semiclassical quantum number. CO: corresponding type of the classical orbit, vibrational (V_i) or rotational (R_i) or ro–vibrational (S^* close to separatrix). SC: semiclassical result. QM: quantum-mechanical result. Π: parity of the quantum-mechanical state.

	$\lambda = 0$					$\lambda = 0.3$		
k	CO	SC $\times 10^{-6}$	QM $\times 10^{-6}$	Π	k	CO	SC $\times 10^{-6}$	QM $\times 10^{-6}$	Π
0	R_1	1.49350	1.49516	e	0	R_1	1.43022	1.43185	e
1	R_1	1.36078	1.36243	o	1	R_1	1.31100	1.31263	o
2	R_1	1.23511	1.23674	e	2	R_1	1.19807	1.19970	e
3	R_1	1.11649	1.11811	o	3	R_1	1.09145	1.09307	o
4	R_1	1.00494	1.00655	e	4	R_1	0.99114	0.99274	e
5	R_1	0.90047	0.90207	o	5	R_1	0.89714	0.89874	o
6	R_1	0.80313	0.80472	e	6	R_1	0.80947	0.81106	e
7	R_1	0.71295	0.71452	o	7	R_1	0.72815	0.72972	o
8	R_1	0.62999	0.63154	e	8	R_1	0.65319	0.65474	e
9	R_1	0.55435	0.55588	o	9	R_1	0.58463	0.58617	o
10	R_1	0.48617	0.48769	e	10	R_1	0.52253	0.52405	e
11	R_1	0.42572	0.42734	o	11	R_1	0.46698	0.46849	o
12	R_1	0.37353	0.37453	e	12	R_1	0.41815	0.41962	e
13	R_1	0.33092	0.33681	o	13	R_1	0.37638	0.37840	o
2	V_3, V_4	0.28257	0.28511	e	14	R_1	0.34258	0.34138	e
			0.27992	o	15	S^*	0.32656	0.32565	o
1	V_3, V_4	0.18726	0.18785	e	1	V_3, V_4	0.27206	0.27285	e
			0.18780	o				0.27233	o
0	V_3, V_4	0.06749	0.68233	e	0	V_3, V_4	0.18879	0.18958	e
			0.68233	o				0.18958	o

1st bifurcation	$\lambda = \sqrt{2}/3$					$\lambda = 0.7$		
k	CO	SC $\times 10^{-6}$	QM $\times 10^{-6}$	Π	k	CO	SC $\times 10^{-6}$	QM $\times 10^{-6}$	Π
0	R_1	1.33746	1.33906	e	0	R_1	1.15146	1.15301	e
1	R_1	1.23850	1.24010	o	1	R_1	1.09727	1.09884	o
2	R_1	1.14475	1.14635	e	2	R_1	1.04613	1.04774	e
3	R_1	1.05621	1.05781	o	3	R_1	0.99809	0.99974	o
4	R_1	0.97287	0.97448	e	4	R_1	0.95321	0.95492	e
5	R_1	0.89475	0.89635	o	5	R_1	0.91156	0.91336	o
6	R_1	0.82183	0.82344	e	6	R_1	0.87327	0.87521	e
7	R_1	0.75412	0.75573	o	7	R_1	0.83853	0.84074	o
8	R_1	0.69162	0.69323	e	8	R_1	0.80767	0.81046	e
9	R_1	0.63433	0.63594	o	9	R_1	0.78143	0.78483	o
10	R_1	0.58225	0.58385	e	10	R_5	0.76253	0.76244	e
11	R_1	0.53537	0.53698	o	11	R_5	0.74009	0.73918	o
12	R_1	0.49371	0.49531	e	12	R_5	0.71197	0.71180	e
13	R_1	0.45725	0.45885	o	13	R_5	0.67967	0.67994	o
14	R_1	0.42600	0.42760	e	14	R_5	0.64373	0.64420	e
15	R_1	0.39996	0.40156	o	15	R_5	0.60441	0.60500	o
16	R_1	0.37912	0.38073	e	16	R_5	0.56189	0.56255	e
17	R_1	0.36350	0.36510	o	17	R_5	0.51626	0.51698	o
18	R_1	0.35308	0.35469	e	18	R_5	0.46761	0.46836	e
19	R_1	0.34787	0.34948	o	19	R_5	0.41598	0.41677	o

Table 3. Energy-level shifts of the $n = 20$ manifold for $\gamma \approx 2.8 \times 10^{-6}$ and different values of λ. Comparison between the semiclassical and quantum-mechanical results. k: semiclassical quantum number. CO: corresponding type of the classical orbit, vibrational (V_i), rotational (R_i) or ro–vibrational (S^* close to separatrix). SC: semiclassical result. QM: quantum-mechanical result. Π: parity of the quantum-mechanical state.

	2nd bifurcation	$\lambda = \sqrt{2/3}$				$\lambda = 1.0$		
k	CO	SC $\times 10^{-6}$	QM $\times 10^{-6}$	Π	k	CO	SC $\times 10^{-6}$	QM $\times 10^{-6}$	Π
0	R_5	1.04128	1.04219	e	0	V_3, V_4	1.47241	1.47397	e
1	R_5	1.03815	1.03906	o				1.47397	o
2	R_5	1.03190	1.03281	e	1	V_3, V_4	1.30633	1.30790	e
3	R_5	1.02253	1.02344	o				1.30790	o
4	R_5	1.01003	1.01094	e	2	V_3, V_4	1.15920	1.16078	e
5	R_5	0.99440	0.99531	o				1.16078	o
6	R_5	0.97565	0.97656	e	3	V_3, V_4	1.03128	1.03288	e
7	R_5	0.95378	0.95469	o				1.03288	o
8	R_5	0.92878	0.92969	e	4	V_3, V_4	0.92312	0.92478	e
9	R_5	0.90065	0.90156	o				0.92478	o
10	R_5	0.86940	0.87031	e	5	V_3, V_4	0.83618	0.83842	e
11	R_5	0.83503	0.83594	o				0.83769	o
12	R_5	0.79753	0.79844	e	12	S^*	0.78125	0.78403	e
13	R_5	0.75690	0.75781	o	13	R_5	0.76473	0.76830	o
14	R_5	0.71315	0.71406	e	14	R_5	0.73227	0.73266	e
15	R_5	0.66628	0.66719	o	15	R_5	0.69394	0.69500	o
16	R_5	0.61628	0.61719	e	16	R_5	0.65088	0.65196	e
17	R_5	0.56315	0.56406	o	17	R_5	0.60361	0.60471	o
18	R_5	0.50690	0.50781	e	18	R_5	0.55243	0.55355	e
19	R_5	0.44753	0.44844	o	19	R_5	0.49754	0.49866	o

	3rd bifurcation	$\lambda = 2/\sqrt{3}$				$\lambda = 1.3$		
k	CO	SC $\times 10^{-6}$	QM $\times 10^{-6}$	Π	k	CO	SC $\times 10^{-6}$	QM $\times 10^{-6}$	Π
0	V_3, V_4	1.93099	1.93281	e	0	V_3, V_4	2.42371	2.42581	e
			1.93281	o				2.42581	o
1	V_3, V_4	1.64974	1.65156	e	1	V_3, V_4	2.02336	2.02547	e
			1.65156	o				2.02547	o
2	V_3, V_4	1.39974	1.40156	e	2	V_3, V_4	1.66773	1.66984	e
			1.40156	o				1.66984	o
3	V_3, V_4	1.18099	1.18281	e	3	V_3, V_4	1.35694	1.35906	e
			1.18281	o				1.35906	o
4	V_3, V_4	0.99349	0.99531	e	4	V_3, V_4	1.09124	1.09338	e
			0.99531	o				1.09338	o
5	V_3, V_4	0.83724	0.83906	e	5	V_3, V_4	0.87118	0.87338	e
			0.83906	o				0.87338	o
6	V_3, V_4	0.71224	0.71406	e	6	V_3, V_4	0.69836	0.70107	e
			0.71406	o				0.70054	o
7	V_3, V_4	0.61849	0.62031	e	7	V_3, V_4	0.58074	0.59153	e
			0.62031	o				0.57099	o
8	V_3, V_4	0.55599	0.55781	e	3	R_1	0.50874	0.50803	e
			0.55781	o	2	R_1	0.44317	0.44429	o
9	V_3, V_4	0.52474	0.52656	e	1	R_1	0.36854	0.36939	e
			0.52665	o	0	R_1	0.28610	0.28733	o

a given $n-$manifold. The comparison with the quantum-mechanical calculations indicates that the "missing state" (*i.e.* eigentrajectory) lies in the close neighbourhood of the separatrix. This effect appears because the states near the separatrix are subjected to quantum mechanical tunnelling [23]. Therefore, within our semiclassical approach, we cannot exactly find and categorise missing semiclassical states.

However, the energy of these missing states labelled with $k = k^*$ can be estimated by taking simply $\epsilon_{n,k^*} = \epsilon_s$, the energy at the separatrix. Then the numerical solution of (17) for ϵ_s gives us an approximate value of k^* for a given "missing state". We name missing states as ro-vibrational states and are denoted by S^* in Tables 2 and 3.

It is important to remark that Tables 2 and 3 show that the structure and evolution of the quantum spectra are easily explained from the semiclassical results, which are nothing else that the reflex of the structure and evolution of the classical phase space. In this sense, the classical vibrational motion is connected with the energy levels of doublet symmetry, while the non-degenerate energy levels are connected with the classical rotational motion. Moreover, the qualitative changes in the energy level spectra as λ varies are the semiclassical/quantum reflex of the bifurcations that take place in the classical counterpart.

Finally, the results obtained in this section can be applied to the case of the generalised van der Waals interaction. In this sense, they provide a complete semiclassical description of that problem, which was partially studied by Ganesan and Lakshamanan [25] with different variables and only for the integrable and near-integrable cases.

5 Conclusions

We present a combined quantum mechanical, classical and semiclassical study of the energy spectrum of a Rydberg hydrogen atom in the presence of uniform magnetic and quadrupolar electric fields when the z component P_ϕ of the angular momentum is zero. Both external fields have been taken as a perturbation to the pure Coulombian system. Owing to the axial symmetry of the problem, the system has two degrees of freedom, and the dynamics is governed by a Hamiltonian depending on a dimensionless parameter λ that represents the relative field strengths.

In the classical analysis, we have performed a Delaunay normalization in order to reduce the problem to a integrable dynamical system where only one degree of freedom is left. We have studied the dynamics arising from the normalised Hamiltonian $\mathcal{H}'_1$ both in cylindrical (ϕ_2, I_2) and spherical (u, v, w) variables, and we have found that: (i) the phase space is made up of two different kind of trajectories: the vibrational and the rotational trajectories. (ii) Depending of the value of λ, we found four different phase flow regimes separated by three oyster bifurcations for $\lambda = (\sqrt{2}/3, \sqrt{2/3}, 2/\sqrt{3})$. (iii) In each regime, the phase space structure is determined by the presence and stability of six isolated equilibria.

In the evolution of the quantum energy spectrum as a function of λ, we have found that the energies of the classical equilibria act like the enveloping of the quantum spectrum, in such a way that the quantum spectrum presents three zones of accumulation around the values of λ for the bifurcations. In other words, the evolution of the energies of the classical equilibria is somehow kind of sketch of the evolution of the quantum spectrum.

From the normalised Hamiltonian $\mathcal{H}'_1$, we have calculated semiclassically the energy levels by means of the EBK quantization rules. These semiclassical results are in very good agreement with quantum results (see Tabs. 2 and 3). From the comparison of semiclassical and quantum results to the classical phase space structure, we find that the vibrational (classical) orbits are connected with the degenerate energy levels of doublet symmetry, while rotational (classical) orbits are connected with non-degenerate energy levels.

In the quantum mechanical calculations, a tiny splitting of the degeneracy appears in the vibrational energy levels near the classical separatrix. This tiny splitting results from tunnelling effects between vibrational states V_3 and V_4 in the vicinity of the separatrix. This splitting does not appear in the semiclassical energy levels because the semiclassical EBK rules do not incorporate the quantum-mechanical tunnelling.

It is worth to note that we have found in this work a deep parallelism between classical and quantum descriptions. This proves again that classical mechanics may be use as a powerful tool in order to get a compact geometric picture of the energy level structure of perturbed Rydberg atoms.

To conclude, although we do not enter into the technical details involved in the possible experimental implementation of the system, we think that the values of the parameters considered in this work would correspond to accessible fields at the laboratory (*e.g.* $\gamma = 2.8 \times 10^{-6}$ corresponds to $B \approx 1.3$ teslas). We leave this question to experimentalists.

References

1. P. Schmelcher, W. Schweizer, *Atoms and Molecules in Strong External Fields* (Plenum Press, New York, 1998); H. Hasegawa, M. Robnik, G. Wunner, Prog. Theor. Phys. Suppl. **98**, 198 (1989)
2. M. Iñarrea, J.P. Salas, V. Lanchares, Phys. Rev. E **66**, 056614 (2002)
3. H. Friedrich, D. Wintgen, Phys. Rep. **183**, 37 (1989); J.I. Martín, V.M. Pérez, A.F. Rañada, Anal. Fis. Ser. A **87**, 48 (1991)
4. G. Baumann, T.F. Nonnenmacher, Phys. Rev. A **46**, 2682 (1992); D. Farrelly, J.E. Howard, Phys. Rev. A **49**, 14094 (1994)
5. Y. Alhassid, E.A. Hinds, D. Meschede, Phys. Rev. Lett. **59**, 1545 (1987)

6. P.A. Braun, E.A. Solov'ev, Sov. Phys. JETP **59**, 38 (1984); P.A. Braun, Rev. Mod. Phys. **65**, 115 (1993)

7. R. Abraham, J.E. Marsden, *Foundations of Mechanics* (Benjamin/Cummings, Reading MA, 1980)

8. A. Deprit, Celest. Mech. **1**, 12 (1969)

9. S.L. Coffey, A. Deprit, B.R. Miller, C.A. Williams, Ann. N.Y. Acad. Sci. **497** 22 (1986)

10. A complementary perturbative study considering both the relative and the center of mass motions of a charged two-body system in a magnetic field is done in W. Becken, P. Schmelcher, Phys. Rev. A **54**, 4868 (1996)

11. A. Deprit, V. Lanchares, M. Iñarrea, J.P. Salas, J.D. Sierra, Phys. Rev. A **54**, 3885 (1996)

12. A. Elipe, S. Ferrer, Phys. Rev. Lett. **72**, 985 (1994)

13. A. Deprit, Celest. Mech. **26**, 9 (1981)

14. B. Goldstein, *Classical Mechanics*, 2nd edn. (Addison-Wesley, Reading MA, 1980)

15. A. Deprit, S. Ferrer, Rev. Acad. Ciencias Zaragoza **45**, 111 (1990)

16. J.E. Howard, R.S. Mackay, Phys. Lett. A **122**, 331 (1987)

17. J.E. Marsden, T.S. Ratiu, *Introduction to Mechanics and Symmetry*, Text in Applied Mathematics **17** (Springer, New York, 1994)

18. M.C. Gutzwiller, *Chaos in Classical and Quantum Mechanics* (Springer–Verlag, Berlin, 1990)

19. M.V. Berry, Proc. *Chaotic Behaviour of Deterministic Systems* (Les Houches Summer School, Session XXXVI) edited by R.H.G. Helleman, R. Stora (North-Holland, Amsterdam, 1983)

20. T.F. Gallagher, *Rydberg Atoms Cambridge*, Monographs on Atomic and Molecular Physics (Cambridge University Press, 1994), Vol. 3

21. A.M. Ozorio de Almeida, *Hamiltonian systems: Chaos and quantization* (Cambridge University Press, 1990)

22. J.B. Delos, S.K. Knudson, D.W. Noid, Phys. Rev. A **28**, 7 (1983); D. Farrelly, K. Krantzman, Phys. Rev. A **43**, 1666 (1991)

23. R.L. Waterland, J.B. Delos, M.L. Du, Phys. Rev. A **35**, 5064 (1987)

24. J.P. Salas, N.S. Simonovic, J. Phys. B: At. Mol. Opt. Phys. **33**, 291 (2000); N.S. Simonovic, J.P. Salas, Phys. Lett. A **279**, 379 (2001)

25. K. Ganesan, M. Lakshmanan, Phys. Rev. A **45**, 1548 (1992)